

Temperature dependent magnetic spin and orbital moments of mass-filtered cobalt clusters on Au(111)

J. Bansmann^{1,a}, A. Kleibert^{2,b}, F. Bulut³, M. Getzlaff³, P. Imperia⁴, C. Boeglin⁵, and K.-H. Meiwes-Broer²

¹ Institut für Oberflächenchemie und Katalyse, Universität Ulm, Albert-Einstein-Allee 47, 89069 Ulm, Germany

² Institut für Physik, Universität Rostock, Universitätsplatz 3, 18051 Rostock, Germany

³ Institut für Angewandte Physik, Universität Düsseldorf, Universitätsstrasse 1, 40225 Düsseldorf, Germany

⁴ Institut für Experimentalphysik, Universität Hamburg, Luruper Chaussee 149, 22761 Hamburg, Germany

⁵ Institut de Physique et de Chimie des Matériaux de Strasbourg, UMR 7504 CNRS-Université Louis Pasteur, 23 rue de Loess, BP 43, 67034 Strasbourg Cedex 2, France

Received 23 February 2007 / Received in final form 22 June 2007

Published online 20 July 2007 – © EDP Sciences, Società Italiana di Fisica, Springer-Verlag 2007

Abstract. Mass-filtered cobalt clusters with a size of 8 nm have been deposited in-situ under soft-landing conditions onto Au(111). The spin and orbital moments of the Co nanoparticles on a Au (111) single crystal have been investigated as a function of the temperature using the element-specific method of X-ray magnetic circular dichroism in photoabsorption. The results hint at an temperature-dependent spin-reorientation transition which is discussed with respect to different contribution to the magnetic anisotropy. Furthermore, by means of an in-situ oxidation experiment, the influence of an exposure to oxygen on the properties of the cobalt clusters has been investigated.

PACS. 73.22.-f Electronic structure of nanoscale materials: clusters, nanoparticles, nanotubes, and nanocrystals – 75.70.-i Magnetic properties of thin films, surfaces, and interfaces – 75.75.+a Magnetic properties of nanostructures – 81.07.-b Nanoscale materials and structures: fabrication and characterization

1 Introduction

The preparation and characterization of metal clusters and nanoparticles are interesting and exciting areas in fundamental research, not at least due to possible technical applications. As a consequence, much effort has been employed to produce size-selected particles by different techniques. Usually, the high surface to bulk ratio and the lower coordination of atoms are the driving forces that lead to size-dependent characteristics. Moreover, even the structural parameters such as the shape of the particles or the interatomic distances are often different from the respective bulk materials, either modified by the fabrication process or by the different thermal equilibrium conditions for small particles. Additionally, the chemical environment, e.g., the substrate, has a huge influence on the physical or chemical properties of these nanomaterials. An overview about such effects and methods for preparation of nanoparticles is given in several review articles [1–8].

In this communication, we will focus our investigation on the magnetic properties of cobalt nanoparticles with diameters of about 8 nm which have been generated in cluster sources and then deposited as preformed particles

onto a gold single crystal surface. This size regime differs from the usual cluster physics regime, where the physical and chemical properties of the respective clusters strongly depend on the exact number of atoms in a particle. In the present case, the nanoparticles consist of several (ten) thousands of atoms. On the other hand, it is even more interesting, that the magnetic properties of such aggregates still show significant deviation from the bulk materials. In particular the magnetic orbital moments can be significantly larger for nanoparticles when compared to the respective bulk value [8,9]. We will present results on the magnetic spin and orbital moments at temperatures between 40 K and 300 K and discuss them with respect to spin-reorientation transitions.

2 Experimental

Experiments on the magnetic properties of exposed cobalt clusters on non-magnetic surfaces require externally applied magnetic fields to saturate the samples. In the present work, we use a superconducting magnet connected to a preparation chamber for in-situ deposition of mass-filtered cobalt nanoparticles at room temperature. The cluster source and the magnet system are mounted at the

^a e-mail: joachim.bansmann@uni-ulm.de

^b e-mail: armin.kleibert@physik.uni-rostock.de

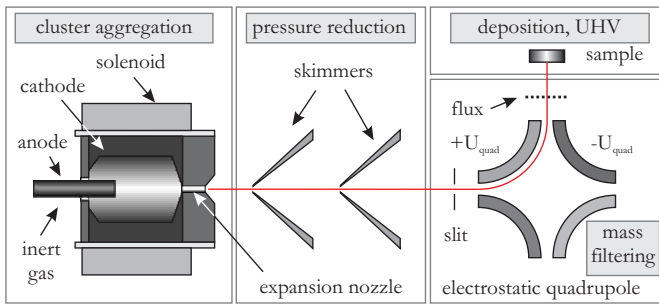


Fig. 1. Schematic drawing of the arc cluster ion source (ACIS) including the mass-separation unit [11].

helical undulator beamline UE46-PGM1 of BESSY. The degree of circular polarization in the third harmonics is $P_{\text{circ}} = 0.9$. X-ray absorption spectra (XAS) are obtained by detecting the total electron yield. With the photon energy tuned to the Co $L_{2,3}$ edges the magnetic spin and orbital moments can be investigated. The superconducting magnet is used to provide constant magnetic fields of up to $B = 1.5$ T parallel to the incoming photon beam. X-ray magnetic circular dichroism spectra (XMCD) are measured at a fixed field while switching the helicity of the impinging radiation for each spectra. The pressure during the experiments is about 5.0×10^{-10} mbar.

The temporal order of our measurements is as follows: First clusters are deposited onto a gold substrate at room temperature (cf. Sect. 2.1). XAS and XMCD spectra are then recorded at room temperature at different angles of incidence: perpendicular to sample surface (referred to as 0°) and at more grazing incidence (40°). Recording one spectra lasts approximately ten minutes. Up to six spectra are recorded for each geometry. The sample is then cooled down to 140 K and the measurements are repeated. Further spectra are subsequently recorded at 40 K. After these experiments the sample is heated to room temperature and the particles are stepwise exposed to 800 L oxygen while recording respective changes in the spectra.

2.1 Cluster source and sample characterization

Cobalt clusters are produced by means of the arc cluster ion source (ACIS), cf. Figure 1. This continuously working source has been developed for a high flux of mass-filtered metal clusters in the 4 nm to 15 nm size regime for in-situ cluster deposition experiments [10, 11]. The cluster source including the mass-filtering unit is fully ultrahigh vacuum compatible and small in size to enable an easy transport to, e.g., synchrotron light sources.

The cluster source consists of several parts: (i) the cluster aggregation part with the hollow cathode made of the target material (here: Co with a purity of 99.9%), (ii) a pumping stage to reduce the large background of noble gas and (iii) a mass-filtering unit. In the presence of a seeding gas at a pressure around 20–40 mbar, the cluster material

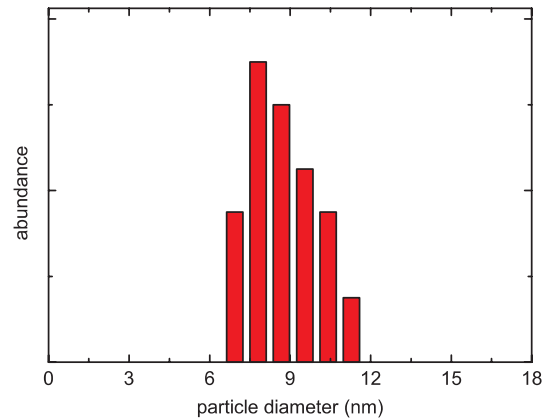


Fig. 2. Size distribution of Co clusters obtained with a pass energy of 1750 eV applied at the quadrupole deflector, cf. Figure 1. The data have been taken from TEM investigations.

is eroded from the hollow cathode using an arc discharge. Small aggregates of this material are kinetically accelerated by collisions in the nozzle and in a weak supersonic expansion to almost the velocity of the seeding gas. The composition of the seeding gas (Ar and He) is controlled by two individual mass flow controllers. After pumping off most of the seeding gas, the fraction of electrically charged nanoparticles in the beam (about 50%, positively and negatively charged with nearly equal contributions) is mass-filtered in an electrostatic quadrupole deflector. The kinetic energy of the clusters is directly related to their mass allowing a separation by using an electrostatic energy dispersive element due to their nearly constant velocity after the expansion in the hollow cathode. Moreover, the kinetic energy of the nanoparticles prior to deposition (usually less than 0.1 eV per atom) is clearly below the fragmentation threshold. The size distribution of the resulting particle deposits has been investigated ex-situ by transmission electron microscopy (TEM) after deposition on a commercial grid, cf. Figure 2. Evaluation of the data yields a narrow size distribution of the deposited clusters without any hint for significant fragmentation. The results displayed in Figure 2 correspond to particles with a mean size of 9 nm. A small amount of larger clusters may occur due to multiply charged particles and a certain velocity slippage. Note that the transport of the samples under ambient conditions results in a partial oxidation of the nanoparticles leading to an increase in the particle diameter. Assuming a reasonable oxide shell thickness of about 2 nm and taking into account the density of CoO, a diameter of about 8 nm for the clean Co nanoparticles prior to air exposure can be inferred. High resolution TEM investigations [11] (not shown here) revealed particles of high crystallinity with fcc structure, in agreement with similar experiments on gas phase generated nanoparticles, see e.g., Kitakami et al. [12]. The equilibrium shape of fcc cobalt particles is obtained by a Wulff construction and yields a truncated octahedron exposing six (001) and eight (111) facets.

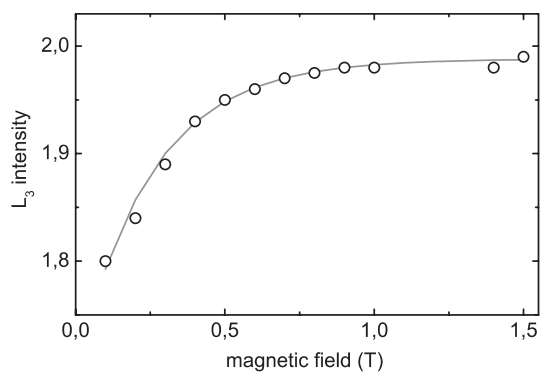


Fig. 3. Magnitude of the L_3 absorption edge of 8 nm cobalt nanoparticles on Au(111) as a function of the applied magnetic field at room temperature, the solid line is a guide to the eye.

3 Results and discussion

Before presenting the orbital and spin moments, we will first show that pure cobalt nanoparticles with a diameter of 8 nm are already magnetically saturated at an external field of $B = 1.5$ T, an important prerequisite for applying the XMCD sum rules (cf. Chen et al. [13]). The XMCD technique and the data evaluation is described later in this article, in the context of Figure 6. For the brief discussion here, please note that the magnitude of the Co L_3 absorption peak is a direct measure for the magnetization of the sample when circularly polarized radiation is used. Figure 3 shows that the intensity (total electron yield) of the Co L_3 photoabsorption edge as a function of the magnetic field remains constant above $B = 1.0$ T. Correspondingly, applying the sum rules yields the magnetic moments in saturation.

In the following we present first the magnetic spin and orbital moments of pure cobalt nanoparticles on gold, cf. Section 3.1. Investigations on cobalt clusters exposed to oxygen are presented later in Section 3.2.

3.1 Mass-filtered clean Co clusters on Au(111) surfaces

Figure 4 displays photoabsorption spectra of Co nanoparticles on a clean Au(111) surface recorded at 40 K. Note that the particle density has been chosen to be below 200 particles per μm^2 in order to avoid significant agglomeration. The data have been recorded in normal incidence at an externally applied magnetic field of $B = 1.5$ T using left and right circularly polarized radiation. The graphs show typical total electron yield spectra taken with left and right circularly polarized radiation (denoted as Y_e^+ and Y_e^- , respectively) of the Co related features on the large Au background. Measuring Au spectra prior to the deposition enables a reliable background subtraction, a prerequisite for the sum rule analysis. A small slope in the Au background at low temperature has been found. The origin of this slope is not arising from a contamination of the Au(111) sample, it is due to oscillations in the

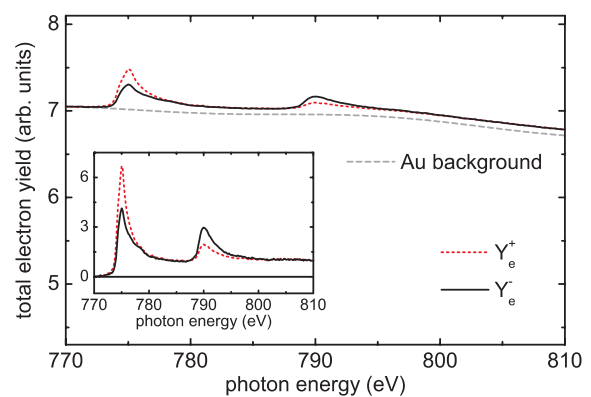


Fig. 4. Total electron yield spectra of 8 nm Co nanoparticles deposited on Au(111) before background subtraction at 40 K. The data in the insets show the corresponding photoabsorption curves after Au background subtraction in the energy regime around the Co $L_{2,3}$ edges at $B = 1.5$ T. All data have been recorded with circularly polarized radiation in normal incidence.

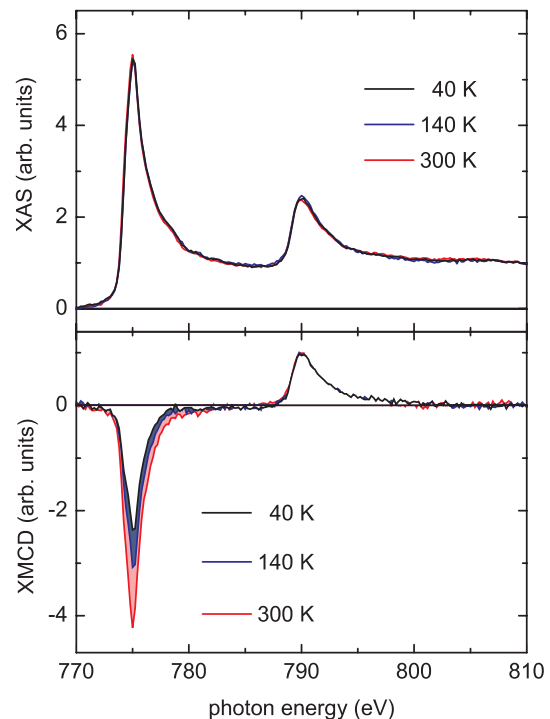


Fig. 5. Upper part: photoabsorption spectra (sum of spectra taken with opposite photon helicities) and related XMCD spectra (lower part) of pure Co nanoparticles as a function of temperature with $B = 1.5$ T. The XMCD spectra in the lower panel have been normalized the Co L_2 edge (peak at 790 eV). The data are recorded in normal incidence (0°).

extended X-ray absorption fine structure (EXAFS) of the Au $N_{2,3}$ edges being more pronounced at low temperature.

The inset of Figure 4 shows the corresponding Co-related photoabsorption spectra at the $L_{2,3}$ edge after background subtraction, the different intensities in the spin-orbit split Co states reflect the magnetization of the particles. This behavior becomes more visible in Figure 5

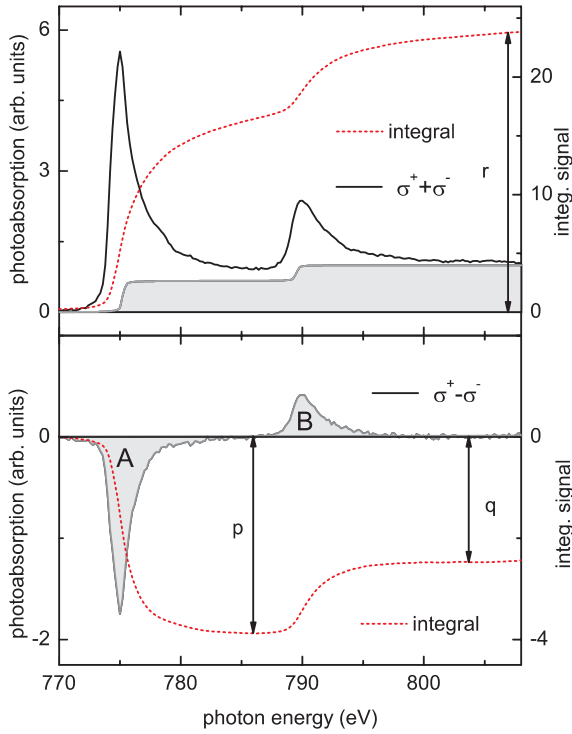


Fig. 6. Sum (upper panel, $\sigma^+ + \sigma^-$) and difference (lower panel, $\sigma^+ - \sigma^-$) of two photoabsorption spectra taken with opposite photon helicity.

where both the sum of the spectra visible in the inset of Figure 4 (top panel) and their intensity differences (bottom) are displayed for different temperatures at normal incidence. Note that the difference spectra have been normalized to 1 at the L_2 edge in order to enhance the visibility of the temperature dependent intensity changes. As explained in detail below the observed variations in the spectra can be attributed to an increase of the magnetic orbital moment when the temperature is raised from 40 K to 300 K.

A quantitative determination of the magnetic orbital m_{orb} and effective spin moments $m_{\text{spin}}^{\text{eff}}$ (in units of μ_B per atom) is achieved by application of magneto-optical sum rules to the experimental spectra [14, 15]. The accordingly calculated integrals of the sum and the difference (cf. upper and lower panel of Fig. 5) of the photoabsorption spectra are displayed in the lower part of Figure 6. The orbital moment, cf. equation (1), is then proportional to the difference of the two areas **A** and **B**, whereas the spin moment, cf. equation (2), is proportional to the sum of area **A** and two times area **B**. To integrate the sum spectra according to the XMCD sum rules, the contribution of excitations into continuum-like final states (shaded area in the upper panel) has to be subtracted. The dashed red lines in both panels denote the integrals, the values p , q and r can be obtained from these curves. Further details on the evaluation of the orbital and spin moments can be found in the original work on the magneto-optical sum rules by Thole et al. [14] and Carra et al. [15] as well as in several review articles (e.g., Chen et al. [13] and

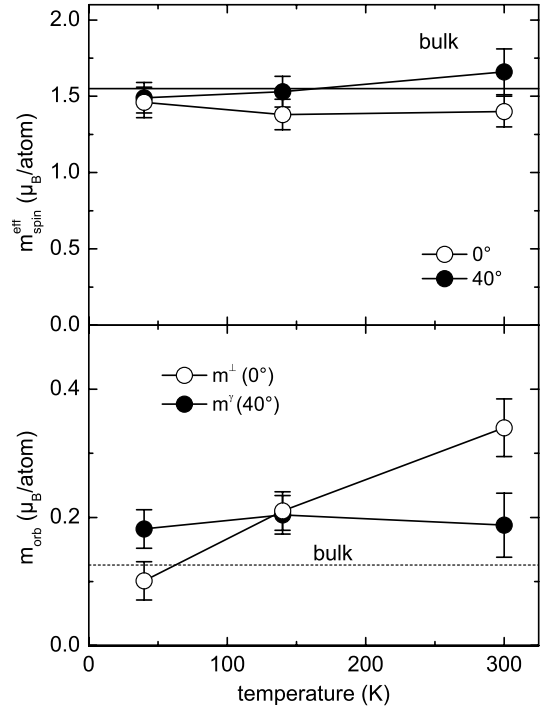


Fig. 7. Spin (top) and orbital moments (bottom) of 8 nm Co nanoparticles on Au(111) as a function of temperature with $B = 1.5$ T, open symbol denote measurements in normal incidence (0°), full symbols at 40° . Horizontal dashed lines indicate the corresponding bulk values of fcc cobalt.

Stöhr et al. [16])

$$m_{\text{orb}} = -4qn_h/3r \propto (A - B) \quad (1)$$

$$m_{\text{spin}} + 7m_T = -(6p - 4q)n_h/r \propto (A + 2B). \quad (2)$$

The number of holes for Co has been set to $n_h = 2.49$, the number of unoccupied states in bulk material [13]. Moreover, the m_{orb} and m_{spin} values have to be corrected for the incomplete degree of circular polarization P_{circ} . The incoming photon beam and the magnetization direction created by the superconducting magnet are always parallel in our setup. It should be mentioned that the determination of the spin moments is influenced by a small contribution from the magnetic dipole term m_T [16–18]. In the following, we will refer to $m_{\text{spin}} + 7m_T$ as an effective spin moment denoted for simplicity as $m_{\text{spin}}^{\text{eff}}$. For cubic crystals the magnetic dipole term is generally small but may be enhanced at the interface. However, due to the supposed statistical orientation of the particles on the surface in our experiment, the magnetic dipole term should cancel out. Since the photoabsorption spectra presented here have been measured by means of total electron yield (TEY), self-absorption effects may result in underestimated spin and orbital moments, for details, see [19, 20]. Based on according simulations for (spherical) Co nanoparticles, we expect to underestimate the spin moments by about 5% and the orbital moment by about 20% in this size regime.

Figure 7 displays the resulting magnetic spin (upper panel) and orbital moments (lower panel) as observed at

temperatures between 40 K and 300 K. Open (filled) circles correspond to data obtained in normal (grazing) incidence, the respective moments are denoted by the superscripts “ \perp ” and “ γ ”. The spin moments in the upper panel show only a slight dependence on the angle of incidence and coincide quite well with bulk-like values for Co as expected for larger clusters. In contrast the magnetic orbital moments (m_{orb}^{\perp} and m_{orb}^{γ} , respectively) reveal a completely different dependence on the temperature when compared to each other. On the one hand, the orbital moments measured at an angle of 40° (m_{orb}^{γ}) are nearly constant (within the error bars) in the whole temperature regime presented here. The absolute value of m_{orb}^{γ} is close to $0.2\mu_B/\text{atom}$ and thus, slightly enhanced with respect to the Co bulk value (cf. dashed line). In normal incidence, on the other hand, we found a pronounced temperature dependence with strongly increasing values from 40 K to 300 K. The main results that can be extracted from Figure 7 are: (i) the value of m_{orb} at 300 K is about twice the Co bulk value; (ii) the orbital moment increases with the temperature; (iii) at 300 K the out-of-plane orbital moment m_{orb}^{\perp} is much larger than the orbital moment m_{orb}^{γ} measured at 40° , whereas the situation is reversed at 40 K.

The high value of $m_{\text{orb}}^{\perp} = 0.34\mu_B/\text{atom}$ at room temperature is remarkable since its value exceeds the Co bulk value by a factor of two. Enhanced orbital moments in Co nanoparticles are well-known for small particles on surfaces, especially for small particles and clusters (consisting of only a few atoms) on surfaces [21–23] as well as for Co impurities in Au host matrices [24], mainly due to low coordination and hybridization effects. For example, Gambardella and coworkers [23] observed an increase of the magnetic orbital moments in this order of magnitude for individual Co atoms and very small clusters on a Pt(111) surface. Significantly enhanced orbital moments of 2D cobalt clusters on Au(111) have been detected by Dürr et al. [21] for clusters below 5 000 atoms. In our experiments, the cobalt particles have a size of about 8 nm being equal to $\sim 27\,000$ atoms. Earlier experiments on Co nanoparticles deposited onto Ni(111) and Fe(110) films, however, only showed orbital moments up to the Co bulk value [11, 25]. It should be mentioned that the hybridization effects between Co clusters and $3d$ -metals such as Fe and Ni are much stronger when compared to the weak hybridization with Au. Cobalt and gold are immiscible and do not form alloys at room temperature. Large orbital moments with values around $m_{\text{orb}} = 0.3\mu_B/\text{atom}$ have also been observed for Co nanoparticles with a height of 2 atomic layers and diameters of up to 7 nm sandwiched into an Au film [22]. However, as these systems are capped with gold, nearly all Co atoms are in direct contact with Au atoms. The symmetry reduction at the Co-Au interface has been made responsible for the high out-of-plane orbital moments, and the values obtained by Koide and coworkers are close to those values predicted by Weller et al. [26] for a monolayer of cobalt embedded between Au(111) and Au layers. The influence of a Au capping layer on the direction of the magnetization is discussed in detail below. For ultrathin films on

Au(111), Pd(111) and Pt(111) surfaces, several authors have observed magnetic orbital moments between 0.2 and $0.3\mu_B/\text{atom}$ which are usually related to a perpendicular magnetization anisotropy [27–29]. Recent results from Luis et al. [30] for small Co clusters on alumina surfaces showed strongly enhanced magnetic anisotropy constants (and enhanced orbital moments) when the particles have been covered with gold or copper. Thus, the magnitude of the magnetic orbital moment for Co nanoparticles on Au(111) itself is not unusual, especially not in case of perpendicular magnetization direction.

The finding, that the orbital moment m_{orb}^{\perp} is larger than m_{orb}^{γ} at room temperature, but smaller at 40 K, could be explained by a temperature-dependent spin reorientation transition (SRT) with in-plane magnetization at low temperature (40 K) and out-of-plane magnetization at room temperature. Please note, that the orbital moments are nearly equal at about 140 K. Indeed, temperature-dependent SRT have been observed for Co films on Au(111) [29, 31], but only in the presence of a thin capping layer. In the above publications the SRT is investigated as a function of the thickness of the Au capping layer or as a function of the thickness of the Co film. Langer and coworkers [29] showed that the magnetization in Co films sandwiched between Au is preferentially aligned to the surface normal at low temperature and in-plane around room temperature when using very thin Au capping layer which coincides with our findings. It should be noted that the Co bulk anisotropy K_1 strongly depends on the temperature and changes its sign at about 200°C , i.e., at low temperatures the c -axis of hcp cobalt is the easy magnetization axis whereas at higher temperatures the magnetization rotates in-plane [32]. Of course, these variations in the magnetic anisotropy result from structural changes in cobalt. Thus, a delicate balance between the competing contributions to the magnetic anisotropy (magneto-crystalline anisotropy, the interface anisotropy, and the shape anisotropy favoring in-plane magnetization) leads to a complicate magnetic behavior of Co films on Au(111). It has been shown in several publications for Co films as well as for small Co clusters [29, 33, 34] that a Au capping layer has a strong influence on the magnetic anisotropy and tends to stabilize a perpendicular magnetic anisotropy. In the case of the experiments presented here, we estimate that our Co nanoparticles are not (or at least not totally) capped by gold since the deposition is performed under soft-landing conditions onto clean Au(111) surfaces without additional cap layer. The contribution from the shape anisotropy which finally determines the in-plane magnetization direction for Co films on Au(111) above 5 ML, is not of importance in the case of separated Co nanoparticles with a size of about 8 nm. Atomic force microscopy and scanning tunneling microscopy results of deposited Co and FeCo nanoparticles on metallic and semiconducting surfaces do not show a strong flattening of the particles upon deposition (no pancake-like shapes) [35, 36]. From the thermodynamic point of view, a capping of cobalt with a very thin Au films is favorable since the surface energy of Co is larger than the

corresponding value for Au. A coating of the surface of the Co particles can, of course, modify its orbital moment significantly. Thus, we cannot completely rule out the possibility that the Co nanoparticles are, to a small degree, capped by gold. However, in the next section we will show that the Co nanoparticles can still be oxidized in the presence of O_2 , first features of a starting cobalt oxide formations could be observed in X-ray photoabsorption after exposure of about 200 L O_2 . Moreover, it has also been shown that the adsorption of molecules from the residual gas, especially CO, onto clean cobalt surfaces can significantly change the magnetic anisotropy (i.e., lowering the magnetic surface anisotropy) and, in an extreme case, can lead to a spin reorientation transition [34,37]. In the case CO adsorption on Co surfaces, usually the perpendicular magnetization anisotropy is stabilized. However, the effects cannot explain the reorientation of the magnetization from out-of-plane to in-plane, since the room temperature measurements have been recorded earlier. Thus, we exclude a significant influence of a CO surface contamination onto our results. This effect would also lead to smaller spin moments when compared to earlier measurements.

Finally, we want to comment on the quite unusual result of an increasing orbital moment with increasing temperature which is in contradiction to theoretical expectations and experimental findings by other groups. There is a general agreement that, as long as no other (e.g., structural or chemical) effects appear at the same time, the orbital moment should decrease with increasing temperature. One could speculate about the possibility that the orbital moment is not completely saturated at low temperature. On the other hand, the decrease of the orbital moment from 300 K to 40 K is quite pronounced and makes this possibility not very realistic. The orbital moment itself is very sensitive to variations in the interatomic distances and thus, tensile or compressive strain could be responsible for a modification in the orbital moment. However, the thermal expansion coefficients for gold and cobalt are nearly identical at room temperature and cannot directly be made responsible for temperature-induced strain. On the other hand, the temperature-dependent magneto crystalline anisotropy of bulk cobalt originates from structural modifications (transition from hcp to fcc with increasing temperature) and might contribute to the unusual behavior of the magnetic orbital moment.

3.2 Influence of oxygen on the magnetic properties of Co clusters on Au(111) surfaces

Earlier experiments on Co nanoparticles on Ni(111) films on W(110) [25] showed a significant influence in both the electronic structure at the Co $L_{2,3}$ absorption edges as well as in the magnitude of the magnetic spin and orbital moments, when exposing the nanoparticles to oxygen. The top panel Figure 8 displays normalized photoabsorption spectra taken in normal incidence at 300 K before and after exposure to 800 L O_2 , the lower panel shows the corresponding XMCD spectra (intensity differences for

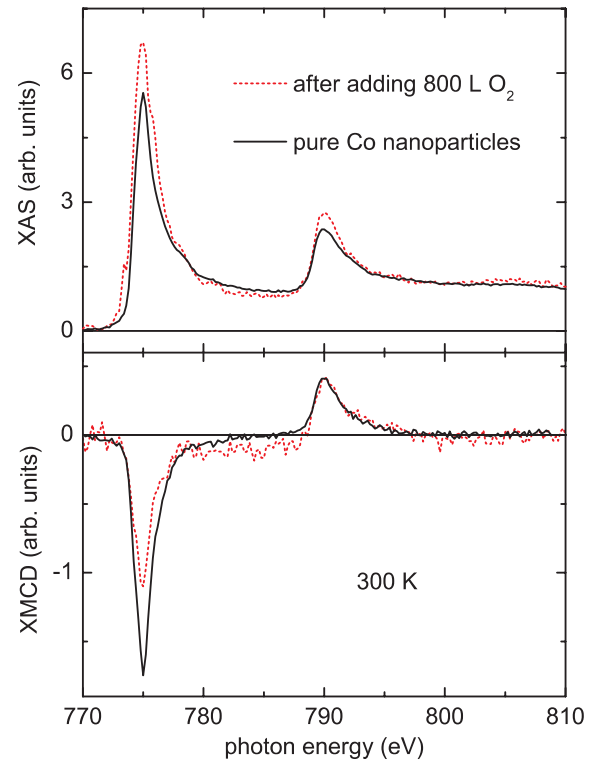


Fig. 8. Upper part: photoabsorption spectra (magnetically averaged) and corresponding XMCD spectra (lower part) for clean and Co nanoparticles exposed to 800 L O_2 . The difference spectra are normalized to the L_2 edge.

opposite photon helicities). After exposure to oxygen the photoabsorption spectra show a significantly increased intensity in the Co peaks and two cobalt oxide (CoO) related contributions (small peaks on both sides of the Co L_3 edge). Both modifications have also been observed in a previous experiment [25]; the higher intensity after exposure to O_2 is caused by an enhancement of the number of holes n_h for cobalt oxide when compared to pure cobalt. The CoO related features clearly show that the nanoparticles are not covered by a gold film. When comparing the peak shape to spectra of pure Co oxide [38], it is evident that the nanoparticles are not completely oxidized, only the outer layers are affected. Most probably, we have a core-shell structure with a pure Co core and CoO at the outside. Related to modifications in the magnetically averaged absorption spectra (upper panel), the magnetic behavior (lower panel), which displays the XMCD spectra, changes after exposure to oxygen. For clean Co nanoparticles on Au(111), we observe higher intensities in the Co L_3 edge when compared to the situation before exposure. Note, that the XMCD spectra have been scaled to identical peak heights in the L_2 peak in order to show the differences in the first peak more clearly. The significantly stronger feature at the Co L_3 (775 eV) resembles a higher ratio of the orbital to the spin moment for the clean sample. This behavior is different to our own results for Co nanoparticles on Ni(111)/W(110) and to findings of other groups where usually an enhanced ratio of the orbital to

the spin moment is observed, see, e.g., Wiedwald et al. [39] and Imperia et al. [40]. It is well-known that the spin moment is reduced upon exposure to oxygen and, moreover, the Co^{2+} ions contribute with higher orbital moments to this ratio. Here, the situation might be different, since we already start from a very high ratio of the orbital to the spin moment for the clean sample (much larger than the ratio reported in [25]). The oxidation process may first modify the physical reason for the enhanced orbital moment at room temperature (e.g., a distortion in the positions of the atom in the outer part of the particle) which would lead to smaller orbital moments. In the next step, the oxidation process might again lead to a higher orbital moment. The presence of a (antiferromagnetic) CoO layer on the nanoparticle usually changes the anisotropy, here, probably to a smaller ratio. However, such effects have to be investigated in the future in more detail.

4 Summary

In conclusion, the magnetic properties of in-situ deposited mass-filtered cobalt nanoparticles on a gold surface have been investigated using a superconducting magnet at the electron storage ring BESSY. X-ray magnetic circular dichroism has been used in order to determine the spin and orbital moments in the 8 nm cobalt nanoparticles. Surprisingly, the Co nanoparticles show an out-of-plane magnetization at room temperature whereas the magnetization is in-plane at 40 K. The possibility of temperature-dependent spin-reorientation transition is discussed with respect to results from Co films and clusters on Au(111) obtained by other groups, with respect to different contribution to the magnetic anisotropy, and with respect to Au capping layers or contamination from the residual gas such as CO and O₂. In-situ oxidation experiments give no evidence for a significant capping of the nanoparticles by gold or adsorbates that could be responsible for the spin reorientation. It is assumed that the balance between the temperature-dependent magneto-crystalline anisotropy of cobalt and the interface anisotropy is responsible for the change in the magnetization direction. The out-of-plane orbital moment m_{orb}^{\perp} at room temperature exceeds the corresponding Co bulk value by a factor of two, but is in agreement with respective values observed for Co in smaller particles and out-of-plane magnetization values for Co films on Au(111) and related surfaces.

We would like to thank our co-workers and colleagues J. Passig, K. Sell (Rostock University). Furthermore, we are indebted to D. Schmitz (Hahn-Meitner-Institut Berlin) for his help during the experiments at the HMI beamline UE-46PGM and to J.-P. Kappler and A. Barla (IPCMS Strasbourg) for their support with respect to the superconducting magnet. We gratefully acknowledge technical support by the staff of BESSY in Berlin, and financial support by the Deutsche Forschungsgemeinschaft (DFG) within the priority program 1153 *Clusters in Contact with Surfaces* (Project Nos. BA 1612/3-2 and GE 1026/4-2).

References

1. K.-H. Meiwes-Broer, *Clusters on surfaces* (Springer-Verlag, Berlin, 2000)
2. U. Kreibig, *Optical properties of metal clusters* (Springer-Verlag, Berlin, 1995)
3. H.J. Freund, Surf. Sci. **500**, 271 (2002)
4. W. Eberhardt, Surf. Sci. **500**, 242 (2002)
5. H. Haberland, *Clusters of atoms and molecules I and II* (Springer-Verlag, Berlin, 1995)
6. H. Brune, Surf. Sci. Rep. **31**, 121 (1998)
7. H.G. Boyen, G. Kästle, K. Zürn, T. Herzog, F. Weigl, P. Ziemann, O. Mayer, C. Jerome, M. Möller, J.P. Spatz, M.G. Garnier, P. Oelhafen, Adv. Funct. Mat. **13**, 359 (2003)
8. J. Bansmann, S.H. Baker, C. Binns, J.A. Blackman, J.-P. Bucher, J. Dorantes-Dávila, V. Dupuis, L. Favre, D. Kechrakos, A. Kleibert, K.-H. Meiwes-Broer, G.M. Pastor, A. Perez, O. Toulemonde, K.N. Trohidou, J. Tuaille, Y. Xie, Surf. Sci. Rep. **56**, 189 (2005)
9. J. Bansmann, A. Kleibert, Appl. Phys. A **80**, 957 (2005)
10. R.P. Methling, V. Senz, E.D. Klinkenberg, T. Diederich, J. Tiggesbäumker, G. Holzhüter, J. Bansmann, K.-H. Meiwes-Broer, Eur. Phys. J. D **16**, 173 (2001)
11. A. Kleibert, J. Bansmann, J. Passig, M. Getzlaff, K.-H. Meiwes-Broer, J. Appl. Phys. **101**, 114318 (2007)
12. O. Kitakami, H. Sato, Y. Shimada, F. Sato, M. Tanaka, Phys. Rev. B **56**, 13849 (1997)
13. C.T. Chen, Y.U. Idzerda, H.J. Lin, N.V. Smith, G. Meigs, E. Chaban, G.H. Ho, E. Pellegrin, F. Sette, Phys. Rev. Lett. **75**, 152 (1995)
14. B.T. Thole, P. Carra, F. Sette, G. van der Laan, Phys. Rev. Lett. **68**, 1943 (1992)
15. P. Carra, B.T. Thole, M. Altarelli, X. Wang, Phys. Rev. Lett. **70**, 694 (1993)
16. J. Stöhr, H. König, Phys. Rev. Lett. **75**, 3748 (1995)
17. R. Wu, A.J. Freeman, Phys. Rev. Lett. **73**, 1994 (1994)
18. C. Ederer, M. Komelj, M. Fähnle, G. Schütz, Phys. Rev. B **66**, 094413 (2002)
19. R. Nakajima, J. Stöhr, Y.U. Idzerda, Phys. Rev. B **59**, 6421 (1999)
20. K. Fauth, Appl. Phys. Lett. **85**, 3271 (2004)
21. H.A. Dürr, S.S. Dhesi, E. Dudzik, D. Knabben, G. van der Laan, J.B. Goedkoop, F.U. Hillebrecht, Phys. Rev. B **59**, R701 (1999)
22. T. Koide, H. Miyauchi, J. Okamoto, T. Shidara, A. Fujimori, H. Fukutani, K. Amemiya, H. Takeshita, S. Yuasa, T. Katayama, Y. Suzuki, Phys. Rev. Lett. **87**, 257201 (2001)
23. P. Gambardella, S. Rusponi, M. Veronese, S.S. Dhesi, C. Grazioli, A. Dallmeyer, I. Cabria, R. Zeller, P.H. Dederichs, K. Kern, C. Carbone, H. Brune, Science **300**, 1130 (2003)
24. W.D. Brewer, A. Scherz, C. Sorg, H. Wende, K. Babelschke, P. Bencok, S. Frota-Pessôa, Phys. Rev. Lett. **93**, 077205 (2004)
25. J. Bansmann, M. Getzlaff, A. Kleibert, F. Bulut, R.K. Gebhardt, K.H. Meiwes-Broer, Appl. Phys. A **82**, 73 (2006)
26. D. Weller, J. Stöhr, R. Nakajima, A. Carl, M.G. Samant, C. Chappert, R. Mégy, P. Beauvillain, P. Veillet, G.A. Held, Phys. Rev. Lett. **75**, 3752 (1995)

27. Y. Wu, J. Stöhr, B.D. Hermsmeier, M.G. Samant, D. Weller, *Phys. Rev. Lett.* **69**, 2307 (1992)
28. D. Weller, Y. Wu, J. Stöhr, M.G. Samant, B.D. Hermsmeier, C. Chappert, *Phys. Rev. B* **49**, 12888 (1994)
29. J. Langer, J.H. Dunn, A. Hahlin, O. Karis, R. Sellmann, D. Arvanitis, H. Maletta, *Phys. Rev. B* **66**, 172401 (2002)
30. F. Luis, F. Bartolomé, F. Petroff, J. Bartolomé, L.M. García, C. Deranlot, H. Jaffrès, M.J. Martínez, P. Bencok, F. Wilhelm, A. Rogalev, N.B. Brookes, *Europhys. Lett.* **76**, 142 (2006)
31. R. Sellmann, H. Fritzsche, H. Maletta, V. Leiner, R. Siebrecht, *Phys. Rev. B* **64**, 054418 (2001)
32. E. Kneller, *Ferromagnetismus* (Springer-Verlag, Berlin, 1962)
33. S. Padovani, F. Scheurer, I. Chado, J.P. Bucher, *Phys. Rev. B* **61**, 72 (2000)
34. M. Dreyer, M. Kleiber, A. Wadas, R. Wiesendanger, *Phys. Rev. B* **59**, 4273 (1999)
35. M. Getzlaff, A. Kleibert, R.P. Methling, J. Bansmann, K.-H. Meiwes-Broer, *Surf. Sci.* **566-568**, 332 (2004)
36. K. Sell, A. Kleibert, V.V. Oeynhausen, K.-H. Meiwes-Broer, *Eur. Phys. J. D*, in press (2007)
37. T. Yokoyama, D. Matsumura, S. Kitagawa, N. Suzuki, T. Ohta, *J. Phys.: Condens. Matter* **15**, S537 (2003)
38. M. Magnuson, S.M. Butorin, J.-H. Guo, J. Nordgren, *Phys. Rev. B* **65**, 205106 (2002)
39. U. Wiedwald, M. Spasova, E.L. Salabas, M. Ulmeanu, M. Farle, Z. Frait, A. Fraile Rodriguez, D. Arvanitis, N.S. Sobal, M. Hilgendorff, M. Giersig, *Phys. Rev. B* **68**, 064424 (2003)
40. P. Imperia, D. Schmitz, H. Maletta, N.S. Sobal, M. Giersig, *Phys. Rev. B* **72**, 014448 (2005)